Research Article

Yuanyuan Liu*

Heavy metals in road dust from typical old industrial areas of Wuhan: Seasonal distribution and bioaccessibility-based health risk assessment

https://doi.org/10.1515/chem-2024-0117
received August 7, 2024; accepted November 14, 2024

Abstract: Heavy metals (HMs) in urban road dust could cause human health risk through potential pathways, especially in industrial areas. To identify pollution sources and propose countermeasures, the seasonal distribution of five HMs (Cu, Cr, Zn, Pb, and Cd) were analyzed from 27 sites of Qingshan Industrial District (QSD) and their induced human health risk was assessed using a developed bioaccessibility-based risk assessment model. Results showed that: (1) The concentrations of five HMs were Zn > Cr > Pb > Cu > Cd. Compared with the background values of each element, the dust enrichment capacity in summer was Zn > Pb > Cd > Cu > Cr, and in winter was Cd > Zn > Pb > Cu > Cr. (2) There was no non-carcinogenic risk in road dust in QSD and children's total non-carcinogenic risk was higher than adults. The non-carcinogenic exposure of each HM was ingested > dermal contact > respiratory inhalation. (3) Cu-Zn-Pb-Cd mainly came from the combined pollution of traffic and industry, and Cr came from the pollution of the steel industry and natural sources. (4) Based on the assessment results, Cr, Zn, Pb, and Cd were determined as the priority control HMs.

Keywords: street dust, health risk, risk management, bioaccessibility, industrial area

1 Introduction

As urbanization progresses rapidly, a majority of the global population now resides in urban areas, exceeding the 50% threshold [1], and urban road dust (also known as atmospheric deposition) is increasingly attracting widespread attention as a major carrier of environmental pollutants. Road dust is both a source of various types of pollutants in the urban environment and a transport medium for pollutants, storing a wide range of pollutants generated by human activities [2]. Due to its porous and irregular structural properties, road dust often contains a variety of heavy metals (HMs). These HMs are typically highly toxic to living organisms and the ecological environment. Additionally, they can enter the human body through the food chain, presenting a potential health risk to humans [3,4]. Studies had shown that HMs could enter the human body through respiration, ingestion, and skin contact, leading to a range of health problems including respiratory diseases, neurological damage, and increased risk of cancer [5–7]. Notably, areas with high traffic density and intensive industrial activity tend to have significantly higher concentrations of HMs compared to other regions [8]. Therefore, it is of great significance to study distribution characteristics and health risks of HMs in road dust in typical old industrial areas for safety of urban ecological environment and human health.

In recent years, many scholars have conducted studies on HMs in urban road dust, exploring their spatial distribution, pollution sources, and health risks [9,10]. These road dust HMs mainly originate from human activities such as automobile emissions, industrial activities, building construction, and daily transportation. Therefore, for areas with high population density, high traffic flow, and dense industry, the content of HMs in road dust may have a high level [11]. In addition, various meteorological factors, such as wind direction, temperature, and rainfall, affected the deposition, distribution, and concentration of HMs in road dust [12]. And according to Bian and Zhu, most of the road dust is comprised of particles smaller than 250 μm, with HMs predominantly concentrated in particles less than 63 μm. So, seasonal variations and dust particle size composition should be under consideration for a scientific exposure risk assessment [13,14]. However, HMs in environmental carriers are not fully absorbed by the human body, which can still result in potential harm. Further, bioaccessibility is another key factor when assessing the health risk of HMs. Bioaccessibility

* **Corresponding author: Yuanyuan Liu**, Hunan Ecological and Environmental Monitoring Center, 410001, Changsha, China, e-mail: hnjjlyy@163.com

refers to the proportion of the metal that is soluble and absorbed in human exposure pathways [15]. For example, when the human body was exposed to road dust, only a fraction of the metal may cross the air-blood barrier of the respiratory system and thus cause damage to human health [16,17]. Therefore, the soluble fraction of HMs in pulmonary fluid could much accurately represent their biological effects doses. Conventional HMs metal assays had mostly focused on total concentrations and neglected their bioaccessibility, which may lead to an undesired overestimation of the actual health risks [18,19]. Therefore, to make a comprehensive consideration of seasonality, dust particle size composition and bioaccessibility differences are of importance during health risk assessment of road dust HMs.

Wuhan city, the capital city of Hubei Province, is an indispensable industrial base in China with a complete industrial production system. Qingshan District (QSD) of Wuhan, a typical area of iron and steel industry, has a permanent population of 458,168 and covers an area of 153.83 km^2. The total GDP in 2023 reached 100.33 billion RMB (1 RMB = 0.14 USD on June 1, 2024), and the secondary industry dominated. Industrial emissions and motor vehicle exhaust emissions obviously caused local environmental pollution issues to some extent [20]. Li et al. conducted a comparison of HM concentrations, including Cd, Cr, Cu, Zn, Ni, and Pb, in the topsoil of urban parks located in Wuhan, Hubei Province. Furthermore, they evaluated the potential health risks for both children and adults through the application of Monte Carlo simulations. The findings indicated that the sources of HMs included a combination of transportation and industrial emissions, as well as natural, agricultural, and other transportation-related sources. Furthermore, the health risks associated with Cd and Cr were particularly concerning for children, given their potential link to cancer risk [21]. Liu et al. evaluated the health risk of HMs from PM2.5 resuspended fugitive dust in Wuhan metropolitan area, and the results showed that transportation-related activities were the main cause of the carcinogenicity risk of Cr due to RFD2.5 [22]. Chen et al. determined the concentrations of HMs (Cr, Mn, Ni, Zn, Fe, Cu, Cd) in street dust in QSD, and evaluated the contamination levels of HMs in street dust by the geo-accumulation method (Igeo) and potential ecological risk assessment [23]. However, as urbanization and industrialization rapidly advance in the region, the anthropogenic influence on urban street dust is intensifying. In addition, the health risk assessment models used in the above studies mostly neglect particle size composition and bioaccessibility differences, which may result in a biased estimation of actual health risk. Hence, a bioaccessibility-based health risk assessment model for the road dust HMs from QSD should be established, and then give targeted risk management policies.

The purposes of this study were: (1) to analyze the seasonal distribution of five HMs (Zn, Cr, Pb, Cu, and Cd) in road dust in QSD; (2) to evaluate HM's potential health risks via improved health risk assessment methods based on their bioaccessibility; (3) to analyze the pollution sources of HMs via multivariate statistical analysis; and (4) to put forward countermeasures and suggestions for prevention and control of HM pollution and health risk management.

2 Materials and methods

2.1 Study area

QSD has a subtropical monsoon climate in the middle and low latitudes. Among the four pillar industries of Wuhan, the two major industries of steel and petrochemicals are in QSD [24]. QSD has evolved into a prominent industrial town, primarily attributed to its eight core industries: metallurgy, chemical manufacturing, environmental protection, electric power generation, machinery production, shipping and logistics, construction services, and building materials [25]. In 2021–2023, the contribution of the secondary industry to local GDP was 61.7, 62.4, and 59.9%, respectively. Meanwhile, some large equipment enterprises are also important components of the city's manufacturing industry. Surrounding these enterprises, there are many communities and schools where most factory workers and their children live and study. HMs produced in the production settled with the dust may threaten residents' health.

2.2 Sample collection and analysis

27 sampling points were set up, numbered S1–S27, according to the purpose of the study and the size of the survey area, on account of the grid layout method of Technical Specifications for Soil Environmental Monitoring (2004) [26], combined with factors such as the annual wind direction rose map of Wuhan, receptors for sensitive people in QSD, and the traffic flow of people and vehicles in and around the main road. And then the latitude and longitude of sampling points were determined, according to the high-precision image in the Baidu map and Gaode map and its latitude and longitude positioning function. The specific location of each sampling point in QSD was determined, and its surrounding landmark buildings for quick positioning were marked.

In the actual sampling process, it is necessary to combine the actual situation of each sampling point and fine-

Figure 1: Distribution of sampling points [27].

tune the position of the sampling point on the premise of ensuring scientific and reasonable distribution. The sampling of road dust in QSD in summer and winter was carried out on a clear and windless day after the local weather remained clear for at least 3 consecutive days. In the sampling process, it is necessary to record the latitude and longitude of each actual sampling point with GPS, and then draw the actual sampling point position diagram, as shown in Figure 1 [27]. In proximity to the sampling point, 3–5 impervious surfaces, each measuring 5 m × 5 m, were randomly chosen. Subsequently, dust samples within the designated area were gathered using a broom, plastic brush, and dustpan. Then, dust samples collected in several areas were screened 10 mesh (2 mm) to remove impurities such as hair, wood chips, gravel, etc., and mixed into one sample, while ensuring that the dust samples collected at each sampling point were at least 0.5 kg. Finally, the collected samples were put into polyethylene zip locks and sealed for storage. The sampling location, number, time, and other information were marked, and environmental characteristics such as traffic conditions, building layout, and greening around the sampling point were recorded.

About 50 g of the original sample after 10 mesh sieve (2 mm) was placed in a zip locking bag for the

determination of pH value, and three-quarters of the sample was used for particle size distribution. The sample sieve was divided into four particle size segments: <62 μm, 62–100 μm, 100–150 μm, and 150–2,000 μm. The contents of organic matter, HM, and bioaccessibility of the first three particle size segments were determined. The above sample processing process was strictly implemented by the relevant demands of China agricultural industry standard "Soil Testing (TY/T 1121)."

Throughout the entire sampling and testing process, we utilized guaranteed reagents for all chemical substances and ultrapure water for all solutions. No metallic tools were used, and all glassware and plastic containers underwent thorough soaking in 10% (v/v) nitric acid (HNO_3) for a minimum of 24 h, subsequently being rinsed multiple times with ultrapure water prior to utilization. To guarantee the precision and dependability of the analytical data, blank samples, duplicate samples, and national standard reference materials (GBW GSS-5) were incorporated into each sample batch. The deviation between duplicate sample sets remained below 5%, and the concentrations of the reference materials fell within the accepted range. As a result, the analytical data adhered to the criteria specified in the "soil environmental quality Risk control standard for soil contamination of agricultural land (GB 15618-2018)" and "Ambient air quality standards (GB 3095-2012)."

2.3 Geoaccumulation index method

Geoaccumulation not only mirrors the natural distribution of HMs in soil but also indicates the influence of anthropogenic activities on their accumulation. In essence, it takes into account the double effects of natural diagenesis and human interventions on HM concentrations in soil [28,29]. The formula is provided below:

$$I_{\log} = \log_2 (C_i/kB_i), \tag{1}$$

where C_i represents the measured concentration of HM i, mg/kg; B_i represents the geochemical background value of i, mg/kg; k is a coefficient applied to adjust for background variations resulting from rock-forming processes, typically assigned a value of 1.5. The HM pollution degree of road dust is divided into seven levels, as shown in Table 1.

2.4 Bioaccessibility-based health risk assessment

The health risk assessment model is widely used both domestically and internationally. In practical applications, health risk assessment models are often associated with different types of uncertainties. Incorporating bioaccessibility into the model can effectively reduce these uncertainties, thereby ensuring that the evaluation results more accurately reflect the actual risk levels. The bioaccessibility of HMs is calculated as follows:

$$C_{\text{bio}} = \frac{C \times V}{m}, \tag{2}$$

$$\text{Bio} = \frac{C_{\text{bio}}}{C_0}, \tag{3}$$

where C_{bio} is the amount of HMs dissolved in the stomach stage; C is the concentration of HM in simulated gastric juice, mg/L; V is the volume of simulated gastric juice, L; m is the amount of soil tested, kg; Bio is the bioaccessibility of HMs in simulated stomach phase, %; C_0 is the total amount of HMs in dust, mg/kg.

Risk of human exposure to HMs in road dust in QSD was evaluated utilizing the exposure risk framework based on the United States Environmental Protection Agency (EPA). There are three types of human exposure to road dust: hand-oral ingestion, respiratory inhalation, and dermal contact, and the five HMs (Cu, Cr, Zn, Pb, and Cd) in this study all have chronic non-carcinogenic risks, while Cr and Cd have carcinogenic risks. The formula for calculating the average daily exposure of HM under different exposure pathways is as follows:

$$\text{ADD}_{\text{ing}} = \frac{C_i \times \text{IngR} \times \text{EF} \times \text{ED}}{\text{BW} \times \text{AT}} \times 10^{-6}, \tag{4}$$

$$\text{ADD}_{\text{inh}} = \frac{C_i \times \text{InhR} \times \text{EF} \times \text{ED}}{\text{PEF} \times \text{BW} \times \text{AT}}, \tag{5}$$

$$\text{ADD}_{\text{dermal}} = \frac{C_i \times \text{SA} \times \text{AF} \times \text{ABS} \times \text{EF} \times \text{ED}}{\text{BW} \times \text{AT}} \times 10^{-6}, \tag{6}$$

$$\text{LADD}_{\text{inh}} = \frac{C_i \times \text{EF}}{\text{PET} \times \text{AT}} \times \left\{ \frac{\text{InhR}_{\text{child}} \times \text{ED}_{\text{child}}}{\text{BW}_{\text{child}}} \times \frac{\text{InhR}_{\text{adult}} \times \text{ED}_{\text{adult}}}{\text{BW}_{\text{adult}}} \right\}, \tag{7}$$

Table 1: Pollution classification of HM

Level	I	II	III	IV	V	VI	VII
I_{geo}	≤0	0–1	1–2	2–3	3–4	4–5	> 5
Pollution degree	Clean	Light pollution	Neutral pollution	Moderate pollution	Heavy pollution	Serious pollution	Severe pollution

where ADD_{ing}, ADD_{inh}, and ADD_{dermal} are the daily exposure amount of hand-oral ingestion, respiratory inhalation, and dermal contact, mg/(kg day), respectively. C_i represents the concentration of HMs by different ingestion routes (mg/kg), this study selected the maximum concentration of HMs extracted from Simulated Gastric Fluid (SBET) as the ingestion concentration for the health risk evaluation across three particle size segments. The concentration of HMs in dust particles smaller than 62 μm was used to represent the respiratory exposure concentration, while the maximum concentration of HMs across all three particle size segments was chosen as the ingestion exposure concentration. IngR is the rate of dust ingestion through hand-oral ingestion, mg/day; InhR is respiration inhalation rate, m^3/day; EF is exposure frequency, day/year; ED is the exposure period, year; BW is the average weight, kg; AT is the average exposure time, day; PEF is dust emission factor, m^3/kg; SA is the surface area of exposed skin, cm^2; AF is the amount of skin adhesion dust, mg/(m^2 day); ABS is a skin absorption factor with no dimension. For carcinogenic effects, an individual's total exposure in childhood and adulthood is evenly distributed over the life cycle. Since the US EPA only gave the carcinogenic slope factor of the respiratory inhalation and did not give the carcinogenic reference value of hand-oral ingestion, and dermal contact, this study only considered the carcinogenic risk of Cr and Cd caused by the respiratory inhalation.

The formula of non-carcinogenic and carcinogenic risks of HMs in road dust is:

$$HQ_{ij} = \frac{ADD_{ij}}{RfD_{ij}}, \tag{8}$$

$$HI_i = \sum_{j=1}^{3} HQ_{ij}, \tag{9}$$

$$CR_i = LADD_i \times SF_i, \tag{10}$$

where HQ_{ij} is the non-carcinogenic risk of HM i under the j exposure pathway; RfD_{ij} is the reference dose of HM i under the j exposure pathway, $mg \cdot kg^{-1} \cdot d^{-1}$; HI_i is the total non-carcinogenic risk of HM i, CR_i is the carcinogenic risk of HM i. SF_i is the carcinogenic risk slope coefficient of HM i, $kg \cdot day \cdot mg^{-1}$. Table S1 shows details about the parameters. When HI < 1, the non-carcinogenic risk of HMs is minimal or can be disregarded. When HI > 1, there exists a notable risk of non-carcinogenic effects associated with exposure to HMs. It is generally believed that when the carcinogenic risk is less than 10^{-6}, the associated risk is negligible, with no significant harm to the human body [30]. However, studies have shown that HMs in environmental carriers are not fully absorbed by the human body, which can still result in potential harm [31]. Furthermore, research indicates that dust particles smaller than 100 μm are more likely to be resuspended by wind, while particles smaller than 62 μm are more readily inhaled by humans. To more rigorously and accurately assess the health risks associated with HMs in road dust, this study selected the maximum concentration of HMs extracted from simulated gastric fluid (SBET) as the ingestion concentration for the health risk evaluation across three particle size segments. The concentration of HMs in dust particles smaller than 62 μm was used to represent the respiratory exposure concentration, while the maximum concentration of HMs across all three particle size segments was chosen as the ingestion exposure concentration. The reference doses and carcinogenic slope factors for the HMs are provided in Table S2.

3 Results and discussion

3.1 Physicochemical properties of HM in QSD

Generally, an alkaline environment promotes the adsorption and precipitation of HMs, while an acidic environment favors their desorption [32]. The overall pH of road dust in QSD was alkaline, significantly exceeding the standard background pH of 6.5 for Chinese soils. The analysis also revealed a slight increase in pH levels from summer to winter. Specifically, in summer, the pH of the dust ranged from 7.37 (S2) to 10.73 (S22), with an average of 8.70. In winter, the pH ranged from 7.60 (S2) to 10.73 (S7), with an average of 9.26.

In QSD, the organic matter content in road dust ranged from 0.47 to 8.32%. Organic matter levels in winter dust were consistently higher compared to those in summer. The average organic matter content in summer dust samples for the three particle size categories were 2.32% (<62 μm), 2.35% (62–100 μm), and 1.67% (100–150 μm), respectively. In winter, the average organic matter content in these same categories were 2.95% (<62 μm), 2.92% (62–100 μm), and 2.41% (100–150 μm), respectively. Notably, the organic matter content in the fine particles (<62 μm) during both summer and winter exceeded the background value of 2% established for China. In both spring and autumn, the organic matter content generally decreased as particle size increased.

3.2 Overview of HM concentrations

The statistical results for HMs content are presented in Table S3. The spatial distribution of HMs concentrations is presented in Figure S1. The concentrations of HMs followed the order: Zn > Cr > Pb > Cu > Cd. However, when

compared to their respective background values, the dust enrichment patterns differed by season: in summer, the order of enrichment was Zn > Pb > Cd > Cu > Cr, while in winter, it was Cd > Zn > Pb > Cu > Cr. Notably, the concentration of Cd across all particle sizes and the concentration of Pb in fine particles were significantly higher in winter compared to summer. The Cu content in winter dust showed a modest increase over summer levels. In contrast, the levels of Cr and Zn in winter dust were similar to those in the summer. Additionally, in summer, the Pb content in larger dust particles was slightly higher than in the finer particles.

The spatial distribution of HMs is illustrated in Figure 1. The distribution of Cu in summer and winter was quite different, and the distribution of Cu in three particle sizes (<62 μm, 62–100 μm, and 100–150 μm) in summer dust was more consistent, mainly concentrated in the western and centra regions of QSD. In winter, Cu in dust with small particle size (<62 μm) and medium particle size (62–100 μm) was mainly located in the south and east, while Cu in dust with large particle size (100–150 μm) was mainly located in the north and east. In summer, Cr in dust with small particle size dust was mainly located in the middle, Cr in dust with medium particle size dust was mainly located in the middle and east, and Cr in dust with large particle size dust was mainly located in the west. The distribution of Cr in the three particle sizes of winter dust was consistent, mainly located in the middle. The percentage of Zn content in the three particle sizes in summer dust exceeded the secondary standard (300 mg/kg) was 66.7, 48.1, and 33.3%, respectively. In the three particle sizes of winter dust, the percentage of Zn content exceeding the secondary standard (300 mg/kg) were 74.1, 51.9, and 37.1%, respectively. In the dust with small particle size, Pb was mainly located in the north and south, while in the dust with large size and medium particle size, Pb was mainly located in the north and west. The distribution of Pb in the three particle sizes of dust in winter was consistent, mainly located in the south. In addition, Pb in dust with small particle size at all sampling sites exceeded the secondary standard (100 mg/kg) in summer. In summer, the areas of Cd in small particle size dust that exceeded the secondary standard (0.6 mg/kg) were S2 (1.975 mg/kg) and S19 (0.636 mg/kg). In large particle size dust, the areas of Cd exceeded the secondary standard (0.6 mg/kg) were S2 (1.271 mg/kg), S19 (1.105 mg/kg), and S26 (0.639 mg/kg). The proportion of Pb exceeding the secondary standard (100 mg/kg) in dust with medium particle size was 40.7%. In the three particle size segments of winter dust, the percentage of Cd content exceeding the secondary standard (0.6 mg/kg) was 96.3, 85.2, and 40.7%.

The geoaccumulation index of HMs was calculated and classified using Formula 1, with the results presented in Table S4. Except for Cr, all HMs in the road dust of QSD exhibited varying degrees of pollution. The extent of HM contamination in the dust was generally more pronounced during winter than in summer. Furthermore, a negative correlation was observed between particle size and the severity of HM pollution: finer road dust particles were associated with higher levels of contamination. In terms of pollution levels, the order of HM contamination in QSD road dust was Zn > Pb > Cd > Cu > Cr in summer, and Cd > Zn > Pb > Cu > Cr in winter.

3.3 Bioaccessibility of HMs

The bioaccessibility contents of HMs are shown in Table 2. The average bioaccessibility of Cu was higher in winter than in summer, and a positive correlation was observed between bioaccessibility and decreasing dust particle size. Similarly, the average bioaccessibility of Cr was also higher in winter. The mean bioaccessibility of Zn in winter and summer was similar.

The mean bioaccessibility of Pb with small particle size (<62 μm) and large particle size (100–150 μm) exhibited notable elevations in winter compared to summer, and the mean bioaccessibility of Pb in middle particle size (62–100 μm) in winter and summer was similar. In summer, the bioaccessibility of HMs in dust was Zn > Cu > Pb > Cd > Cr, and in winter, the bioaccessibility of HMs in dust was Cu > Cd > Zn > Pb > Cr.

3.4 Bioaccessibility-based improved health risk

In this study, the maximum concentration of HMs extracted from simulated gastric juice (SBET) in three particle sizes was designated as the intake concentration. The HM concentration in small particle size (<62 μm) was chosen as the respiratory concentration, and the maximum concentration of HMs in three particle sizes was considered as the intake concentration. The Bioaccessibility-based health risk value of HM was calculated and is detailed in Table S5.

3.4.1 Spatial distribution of non-carcinogenic risk

The geographical dispersion of the total non-carcinogenic risk of HMs was illustrated in Figure 2. The average non-carcinogenic risk associated with each HM fell below 1,

Table 2: Bioaccessibility ratio of road dust in QSD (%)

HM	Partical size	Summer					Winter				
		MIN	MAX	MEAN	SD	CV	MIN	MAX	MEAN	SD	CV
Cu	<62	10.49	51.43	32.72	11.46	35.03	33.50	88.86	60.66	14.19	23.38
	62–100	13.67	86.0	34.23	16.07	46.95	21.38	71.30	46.54	13.57	29.16
	100–150	7.0	84.09	28.97	19.97	68.93	9.29	92.79	39.52	19.00	48.08
Cr	<62	1.03	14.19	4.54	2.88	63.40	7.96	25.07	15.65	5.11	32.66
	62–100	1.37	12.49	5.89	3.43	58.15	3.49	23.00	12.44	4.95	39.81
	100–150	1.66	17.60	7.03	3.86	54.87	5.20	36.50	13.59	8.13	59.87
Zn	<62	19.66	71.87	53.98	12.35	22.88	28.85	60.11	49.26	9.24	18.76
	62–100	21.11	86.49	51.50	16.40	31.85	26.86	62.10	45.29	9.02	19.91
	100–150	24.29	76.79	52.82	14.03	26.56	25.54	70.14	44.19	10.79	24.42
Pb	<62	6.75	32.29	12.87	5.77	44.80	13.32	70.02	38.76	18.99	48.99
	62–100	12.30	64.88	31.54	11.19	35.50	19.48	70.25	37.28	14.43	38.70
	100–150	6.08	51.31	19.66	11.45	58.21	10.15	69.50	36.52	14.90	40.79
Cd	<62	5.64	46.97	22.16	10.90	49.19	12.39	86.07	56.34	21.85	38.77
	62–100	9.04	27.55	17.14	5.54	32.35	10.34	84.75	49.67	17.28	34.79
	100–150	3.50	35.88	12.43	6.54	52.63	16.52	82.02	45.01	17.15	38.11

signifying the overall non-carcinogenic level of each HM was low, which was like the results of another study [33]. The primary route of non-carcinogenic exposure to each HM was ingestion, surpassing dermal contact and respiratory inhalation, emphasizing the significance of ingestion as the dominant non-carcinogenic exposure pathway for HMs. In addition, the cumulative non-carcinogenic risk of HMs was notably elevated in children. The risk contribution rate of HMs in children was Pb (46.85%) > Cr (43.83%) > Zn (3.61%) > Cu (3.11%) > Cd (2.60%). The risk of HMs in adults was Cr (52.47%) > Pb (39.43%) > Zn (2.95%) > Cd (2.63%) > Cu (2.51%), indicating that Cr and Pb exerted a more pronounced non-carcinogenic impact on human. The non-carcinogenic effects of Cu were widespread, mainly affecting the western, central, and northern parts. The non-carcinogenic effects of Cr were mainly concentrated in the central and northern parts. The non-carcinogenic effects of Zn and Pb were mainly concentrated in the southern part, with some effects in the eastern part. The non-carcinogenic effects of Cd were mainly located in the south and have some effects in the west.

3.4.2 Spatial distribution of carcinogenic risk

The distribution of carcinogenic risk is shown in Figure 3. The carcinogenic risk associated with Cr and Cd ranged from 3.39×10^{-7} to 1.31×10^{-6} and from 3.35×10^{-10} to 1.09×10^{-9}, respectively. The mean carcinogenic risks for Cr and Cd were 5.87×10^{-7} and 5.31×10^{-10}, respectively, indicating that Cd in QSD did not pose a significant carcinogenic risk. However, the carcinogenic risk of Cr exceeded 10^{-6} at certain points, suggesting a significant carcinogenic risk at these locations. Notably, significant carcinogenic risks for Cr were observed at the S16 (1.13×10^{-6}) and S22 (1.31×10^{-6}) points. The carcinogenic risks for Cr were primarily concentrated in the central and eastern regions, while those for Cd were mostly located in the western and northern

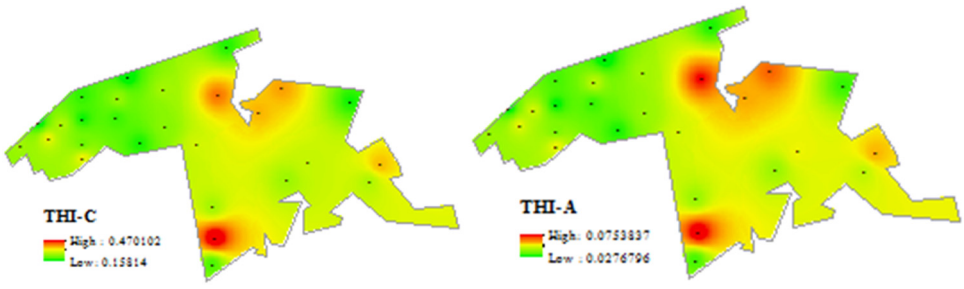

Figure 2: Spatial distribution of total non-carcinogenic risk of HMs in QSD.

regions. The variation coefficients for the carcinogenic risk values of Cr and Cd were 40.39 and 38.67%, respectively, indicating moderate variability, which suggests they are influenced by certain human activities.

Compared to classical health risk assessments, which only consider the carcinogenic risks of HMs through the respiratory pathway, the improved health risk assessment method in this study considers the concentration of HMs in particles with a size of less than 62 μm. In classical health risk assessments, the exposure concentration is based on the average amount of HMs in the environment. In contrast, the improved assessment method focuses on the concentration of HMs in fine particles (<62 μm), which are more likely to be inhaled and thus pose a greater health risk. Previous studies [34] have shown that the HM content in street dust is inversely correlated with dust particle size. Therefore, when evaluating the carcinogenic risk of HMs in street dust, the classical risk assessment tends to underestimate the actual risk, as it does not account for the higher concentrations of HMs in finer, inhalable particles. From some published studies home and aboard, classical risk assessments based solely on the total concentration of HMs tend to be overly conservative [35]. Ma et al. [36] compared the bioaccessibility of HMs in dust and soil in Lanzhou City and found that, during the stomach phase, the bioaccessibility of HMs was higher in both dust and soil compared to the intestinal phase. Additionally, the bioaccessibility of HMs in dust and soil during the stomach phase was greater than that in the topsoil. Both Huang [37] and Wu's [38] studies showed that the traditional risk assessment may lead to a higher risk value.

3.4.3 Priority control of HMs and regions

Compared with the background values of each element, the orders of dust enrichment capacity in summer and winter were Zn > Pb > Cd > Cu > Cr and Cd > Zn > Pb > Cu > Cr. For Cu, the priority control areas in summer were S11, S21, and S23, and in winter were S4 and S19. For Cr, the priority control areas in summer were S4, S11, S21, S22, and S23, and in winter was S16. The HM concentration and the relative enrichment degree of Zn were high, and Zn should be strictly controlled except for a few points. In summer, the concentration levels of Pb surpassed those observed in winter, and Pb in small particle size of all the sampling points in summer exceeds the national secondary standard. The priority control areas of Pb in winter were S6, S11, S12, S15, S16, S19, S20, S23, and S26. For Cd, the priority control areas in summer were S2, S4, S8, S11, S12, S14, S15, S18, S19, S20, S21, and S26. In winter, the concentration and the relative enrichment degree of Cd were high, except for S22. The Cd of all sampling points exceeded the national secondary standard. In summary, compared with the national secondary standard, Zn, Pb, and Cd were the priority HMs, and there were cases of exceeding the standard in the whole QSD. Based on the geo-accumulation index analysis, Zn, Pb, and Cd were the priority HMs. The health risk assessment pinpointed Cr and Pb as the priorities for control measures, and the priority control areas were concentrated in S16, S19, S21, S22, and S26.

3.5 Source apportionment of HMs

3.5.1 Correlation analysis of HMs in road dust

SPSS software was used to calculate the Pearson correlation coefficient of HM, and the results are shown in Table 3.

At the level of 0.01, a notable association was observed between Cu, Zn, and Pb, as well as among Cu, Zn, and Cd, suggesting a commonality in their pollution sources or the presence of combined pollution that involves these HMs, which was like the study of Chai et al. [39]. If there was a correlation between Cr and Zn and Pb, but no correlation with Cu and Cd, it indicated that the source of Cr may be distinct from that of the other elements.

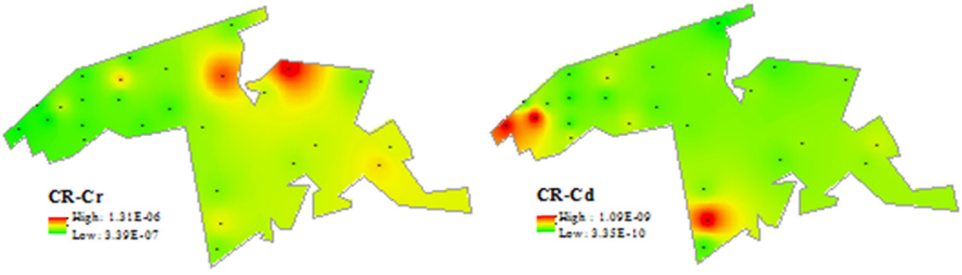

Figure 3: Spatial distribution of Carcinogenic risk of Cr and Cd in QSD.

Table 3: Pearson correlation coefficient of HM

HM	Cu	Cr	Zn	Pb	Cd
Cu	1				
Cr	0.122	1			
Zn	0.339**	0.171*	1		
Pb	0.286**	0.181*	0.444**	1	
Cd	0.308**	0.042	0.495**	0.140	1

*$p < 0.05$; **$p < 0.01$.

3.5.2 Principal component analysis (PCA) of HMs in road dust

PCA serves as an effective method for diminishing the extensive overlap of information between variables while maintaining minimal loss of data integrity, within the confines of a reduced, high-dimensional variable space. This technique has been widely used. The Kaiser-Meyer-Olkin (KMO) test serves as a prerequisite for conducting PCA, with a KMO statistic below 0.5 suggesting unsuitability for PCA application. In this study, a KMO test value of 0.634 was obtained, validating the appropriateness for PCA, and the ensuing PCA results are presented in Table 4.

The results of PCA showed that principal components with two eigenvalues greater than 1 contributed 61.87% of the total variables, signifying that these two principal components could encapsulate the majority of the information of the whole data. Principal component 1 contributed 41.703% and principal component 2 contributed 20.167% of the total variable. Principal component 1 consisted of Cu, Zn, Pb, and Cd, and their load on principal component 1 were 0.655, 0.826, 0.652, and 0.660, respectively. Principal component 2 contained Cr, and its load on principal component 2 was 0.803. Principal component 1 was mainly influenced by human sources, while principal component 2 was mainly from natural sources.

3.5.3 Cluster analysis of HMs in road dust

SPSS was used for hierarchical clustering analysis (CA) of HM data, and the results are shown in Figure 4. Cr and other HMs were clustered into a class at a distance of 25, so HMs can be divided into two categories, the first category included Cu, Zn, Pb, and Cd, these four HMs had a strong correlation, especially Zn and Cd. The second category was Cr, its correlation with other elements was very weak. The results of hierarchical CA were like those of correlation analysis and PCA.

Cu concentration in street dust within QSD was highest in the western region, where the traffic network is more developed, and traffic flow is significant. It is hypothesized that the Cu primarily originates from automobile exhaust emissions, the corrosion of vehicle metal parts, and brake material wear. The distribution of Zn in the street dust was more widespread, with higher concentrations in the west, again linked to the high traffic density, and possibly influenced by automobile exhaust, tire wear, and aging. In the eastern part of QSD, which is more industrialized and experiences frequent large truck traffic, Zn levels may be associated with tire and body wear from heavy vehicles. Pb contamination in the street dust indicated combined pollution sources from both traffic and industrial activities. The unusually high Pb concentrations around sampling points S17 and S19 can be attributed to nearby industrial facilities, such as the Qingshan Shipyard of China Long Hang Shipbuilding Industry Corporation, along with surrounding petrochemical, mechanical, and building material companies, as well as railway systems. Cd concentrations were notably high at

Table 4: Main results of HM PCA in QSD

Project	First principal component	Second principal component
Characteristic value	2.09	1.01
Rate of contribution (%)	41.70	20.17
Cumulative contribution rate (%)	41.70	61.88
Cu	0.66	−0.09
Cr	0.34	0.80
Zn	0.83	−0.11
Pb	0.65	0.31
Cd	0.66	−0.50

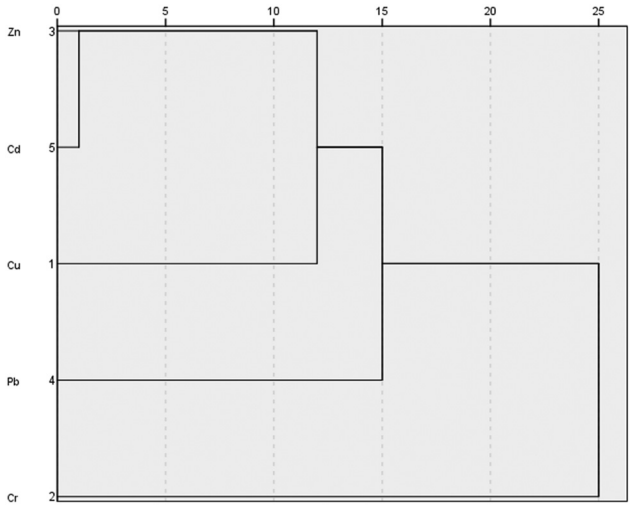

Figure 4: CA of HM levels.

sampling points S2 and S19. S2 is located near a school with a high number of students, a busy bus stop, and surrounding commercial areas, which contribute to increased traffic. S19 is situated near a railway, overhead structures, and a heavily trafficked area, with a concentration of mechanical and electrical companies, and steel manufacturing facilities. It is thus speculated that Cd pollution in the street dust of QSD arises primarily from automobile exhaust, tire wear, and industrial activities. Cr concentrations in street dust were relatively low compared to background levels, and there was little seasonal variation between summer and winter, suggesting that Cr in the district's street dust was predominantly from natural sources. However, higher concentrations at specific points, such as S16 and S21, may be influenced by industrial emissions, particularly from nearby Wuhan Iron and Steel Group. Overall, the findings indicated that Cr in the street dust of QSD originates from a combination of steel industry emissions and natural sources. Therefore, according to the comprehensive analysis of Pearson correlation analysis, PCA and CA, Cu-Zn-Pb-Cd mainly came from the combined pollution of traffic and industry, and Cr came from the pollution of the steel industry and natural sources.

4 Conclusion

The study investigated the content levels, seasonal variations, and spatial distribution characteristics of HMs in road dust in QSD, while assessing potential health risks associated with these metals using a bioaccessibility-based health risk assessment method. The results revealed that Cd exceeded safety limits more significantly in both summer and winter, with its concentration patterns showing greater consistency, primarily in the western and southern regions. HM pollution (excluding Cr) varied in intensity, with higher pollution levels observed in winter. Overall, the extent of HM contamination was inversely related to the particle size of the road dust. The Cu-Zn-Pb-Cd pollution was mainly attributed to the combined influence of traffic emissions and industrial activities, while Cr pollution stemmed primarily from the iron and steel industry as well as natural sources. Based on these findings, several targeted risk control measures were proposed: (1) accelerating the industrial transformation of QSD by fostering clean, energy-efficient, and low-emission emerging industries; (2) enhancing source control and pollutant discharge regulations; (3) establishing a comprehensive environmental health risk monitoring system; and (4) promoting environmental and health education, strengthening information transparency, and increasing public engagement. Furthermore, given the close relationship between dust, soil, and atmospheric particles, the migration and transformation of HMs in urban street dust warrants further investigation.

Funding information: Author state no funding involved.

Author contributions: Methodology and writing; Yuanyuan Liu.

Conflict of interest: The author has no conflicts of interest to declare.

Data availability statement: All the data created or analyzed during this research is contained in this published article and its supporting material files.

References

[1] Jiang P, Gao C, Zhao JR, Li F, Ou CH, Zhang T, et al. An exploration of urban air health navigation system based on dynamic exposure risk forecast of ambient PM2.5. Environ Int. 2024;190:108793.
[2] Men C, Liu R, Xu F, Wang Q, Guo L, Shen Z. Pollution characteristics, risk assessment, and source apportionment of heavy metals in road dust in Beijing, China. Sci Total Environ. 2018;612:138–47.
[3] Masih J, Gautam S, Nair A, Singhal RK, Venkatesh M, Basu H, et al. Chemical characterization of sub-micron particles in indoor and outdoor air at two different microenvironments in the western part of India. SN Appl Sci. 2019;1:165.
[4] Gupta V, Bisht L, Arya AK, Singh AP, Gautam S. Spatially resolved distribution, sources, exposure levels, and health risks of heavy metals in <63 μm size-fractionated road dust from Lucknow City, North India. Int J Environ Res Public Health. 2022;19(19):12898.
[5] Gautam S, Talatiya A, Patel M, Chabhadiya K, Pathak P. Personal exposure to air pollutants from winter season bonfires in rural areas of Gujarat, India. Expo Health. 2020;12(1):89–97.
[6] Liu Z, Cai L, Liu Y, Chen W, Wang Q. Association between prenatal cadmium exposure and cognitive development of offspring: A systematic review. Environ Pollut. 2019;254:113081.
[7] Kumar RP, Perumpully SJ, Samuel C, Gautam S. Exposure and health: A progress update by evaluation and scientometric analysis. Stoch Environ Res Risk Assess. 2023;37(2):453–65.
[8] He Y, Peng C, Zhang Y, Guo Z, Xiao X, Kong L. Comparison of heavy metals in urban soil and dust in cities of China: Characteristics and health risks. Int J Environ Sci Technol. 2023;20(2):2247–58.
[9] Hou S, Zheng N, Tang L, Ji X, Li Y, Hua X. Pollution characteristics, sources, and health risk assessment of human exposure to Cu, Zn, Cd and Pb pollution in urban street dust across China between 2009 and 2018. Environ Int. 2019;128:430–7.
[10] Gupta V, Bisht L, Deep A, Gautam S. Spatial distribution, pollution levels, and risk assessment of potentially toxic metals in road dust from major tourist city, Dehradun, Uttarakhand India. Stoch Environ Res Risk Assess. 2022;36(10):3517–33.
[11] Gogoi N, Sarma A, Choudhury M, Samanta P, Faizan M, Sadhak S. Soil heavy metal pollution and ecological risk assessment in disturbed and undisturbed soil of Morigaon, Assam. Discov Environ. 2024;2(1):13.

[12] Wang X, Gao Q, Wang W, Yan J, Liu Y, Kuang S, et al. Determining priority control factors for heavy metal management in urban road dust based on source-oriented probabilistic ecological-health risk assessment: A study in Xi'an during peak pollution season. J Environ Manage. 2024;369:122105.
[13] Bian B, Zhu W. Particle size distribution and pollutants in road-deposited sediments in different areas of Zhenjiang, China. Environ Geochem Health. 2009;31:511–20.
[14] Yang Y, Lu X, Yu B, Wang Z, Wang L, Lei K, et al. Exploring the environmental risks and seasonal variations of potentially toxic elements (PTEs) in fine road dust in resource-based cities based on Monte Carlo simulation, geo-detector and random forest model. J Hazard Mater. 2024;473:134708.
[15] Zupančič M, Miler M, Žibret G. The relationship between the inhalation bioaccessibility of potentially toxic elements in road dust from a heavily polluted industrial area and the source of their pollution. Environ Pollut. 2024;361:124810.
[16] Wiseman CLS, Zereini F. Characterizing metal(loid) solubility in airborne PM10, PM2.5 and PM1 in Frankfurt, Germany using simulated lung fluids. Atmos Environ. 2014;89:282–9.
[17] Yang ZY, Liu H, Li JY, Bao YB, Yang J, Li L, et al. Road dust exposure and human corneal damage in a plateau high geological background provincial capital city: Spatial distribution, sources, bioaccessibility, and cytotoxicity of dust heavy metals. Sci Total Environ. 2024;912:169140.
[18] Liu X, Ouyang W, Shu Y, Tian Y, Feng Y, Zhang T, et al. Incorporating bioaccessibility into health risk assessment of heavy metals in particulate matter originated from different sources of atmospheric pollution. Environ Pollut. 2019;254:113113.
[19] Ren Y, Luo Q, Zhuo S, Hu Y, Shen G, Cheng H, et al. Bioaccessibility and public health risk of heavy metal(loid)s in the airborne particulate matter of four cities in northern China. Chemosphere. 2021;277:130312.
[20] Liu ZY, Cheng JL, Li CY, Gao Y, Zhan CL, Liu S, et al. Pollution characteristics and source apportionment of carbonaceous components in road dust from Qingshan District of Wuhan. Environ Chem. 2021;40(3):772–8.
[21] Li D, Lu Q, Cai L, Chen L, Wang H. Characteristics of soil heavy metal pollution and health risk assessment in urban parks at a megacity of Central China. Toxics. 2023;11(3):257.
[22] Liu S, Zhan C, Zhang J, Guo J, Liu H, Liu T, et al. Source-specific health risk assessment of PM2.5 bound heavy metal in re-suspended fugitive dust: A case study in Wuhan metropolitan area, central China. J Clean Prod. 2022;379:134480.
[23] Chen H, Zhan C, Liu S, Zhang J, Liu H, Liu Z, et al. Pollution characteristics and human health risk assessment of heavy metals in street dust from a typical industrial zone in Wuhan City, Central China. Int J Environ Res Public Health. 2022;19(17):10970.
[24] Chen CY, Li F, Du HZ, Liu XL, Liu SQ, Zhang JD. Fuzzy health risk assessment and integrated management of toxic elements exposure through soil-vegetables-farmer pathway near urban industrial complexes. Sci Total Environ. 2021;764:142817.
[25] Chen H, Zhan CL, Liu S, Zhang JQ, Liu HX, Liu ZG, et al. Pollution characteristics and human health risk assessment of heavy metals in road dust from a typical industrial zone in Wuhan City, Central China. Int J Environ Res Public Health. 2022;19(7):10970.
[26] Ministry of Ecology and Environment of the People's Republic of China. The Technical Specification for soil Environmental monitoring (HJ/T 166-2004). Beijing: Ministry of Ecology and Environment of China; 2004 (in Chinese).
[27] Chen H, Zhan CL, Liu S, Zhang JQ, Liu HX, Liu ZG, et al. Pollution characteristics and human health risk assessment of heavy metals in street dust from a typical industrial zone in wuhan City, Central China. Int J Environ Res Public Health. 2022;19(17):10970.
[28] Zhan YZ, Jiang X, Chen CX, Gao HG, Jin XC, Li C, et al. Spatial distribution characteristics and pollution assessment of heavy metals in sediments from the southwestern part of Taihu Lake. Res Environ Sci. 2011;24(4):363–70 (in Chinese).
[29] Zhao JT, Wu EW, Zhang B, Bai X, Lei P, Qiao XW, et al. Pollution characteristics and ecological risks associated with heavy metals in the Fuyang river system in North China. Environ Pollut. 2021;281:116994.
[30] Fei XF, Lou ZH, Xiao R, Ren ZQ, Lv XN. Source analysis and source-oriented risk assessment of heavy metal pollution in agricultural soils of different cultivated land qualities. J Clean Prod. 2022;341:130942.
[31] Ruby MV, Davis A, Schoof R, Eberle S, Sellstone CM. Estimation of lead and arsenic bioavailability using a physiologically based extraction test. Environ Sci Tech. 1996;30(2):422–30.
[32] Xiao MS. Fuzzy comprehensive risk assessment and management of heavy metals in sediments from the Honghu Lake. Wuhan: Zhongnan University of Economics and Law; 2018 (in Chinese).
[33] Jiao W, Niu Y, Li B, Duan YJ, Zhang N, Zhao YM, et al. Health risk assessment and anthropogenic source identification of heavy metals in urban road dusts based on chemical fraction analysis. J Ecol Environ. 2018;27(12):2269–75 (in Chinese).
[34] Chang J, Liu M, Li XH, Lin X, Wang LL, Gao L. Fractionation and bioavailability of heavy metal contamination of urban surface dusts in Shanghai City. Environ Sci. 2008;29(12):3489–95 (in Chinese).
[35] Feng KH, Fan J, Hii LUS, Luo QS, Cao XD, Xu XY. Human health risk assessment of heavy metals in soil from a smelting plant based on bioaccessibility. China Environ Sci. 2021;41(1):442–50 (in Chinese).
[36] Ma XY, Xia DS, Liu XY, Liu H, Fan YX, Chen PY, et al. Application of magnetic susceptibility and heavy metal bioaccessibility to assessments of urban sandstorm contamination and health risks: Case studies from Dunhuang and Lanzhou, Northwest China. Sci Total Environ. 2022;830:154801.
[37] Huang CC. Contamination characteristic and risk analysis of heavy metals in street dust in Wuhan City, Hubei Province. Hubei: Yangtze University; 2022 (in Chinese).
[38] Wu M. Particle size effect and health risk assessment of heavy metals in street dust in Wuhan City. Hubei: Yangtze University; 2023 (in Chinese).
[39] Chai SW, Wen YM, Zhang YN, Dong HY, Chen YJ, Long XB, et al. The heavy metal content character of agriculture soil in Guangzhou suburbs. China Environ Sci. 2003;23(6):592–6 (in Chinese).